Exposure Synchronization in Optical Camera Communications for Time Division Multiplexing

Hiroaki Matsunaga, *Student Member, IEEE*, Tomohiro Yendo, Shintaro Arai, *Member, IEEE*, and Takaya Yamazato, *Senior Member, IEEE*

***Abstract*—Optical camera communication (OCC) is a type of visible light communication that employs a camera as the receiver. Various flicker-free OCC methods using a general-purpose low-frame rate camera have been proposed. In particular, the undersampling method uses a short exposure camera and a light-emitting diode that blinks faster than the camera's frame rate. Despite the short exposure time, the transmitter has to send a symbol for a frame period or longer because the relationship between the symbol timing of the transmitter and exposure timing of the receiver is indeterminate. We propose resolving this indeterminacy by synchronizing the exposure timing to the transmitter. In the proposed method, the transmitter sends multiple data channels in a frame period by time division multiplexing, and the receiver selects a channel. Then, a single symbol of multilevel phase shift keying is extracted from a single pixel value in a frame. Experiments confirmed that the exposure timing could be synchronized even with a degraded signal–noise ratio and that the receiver could select the desired channel. The proposed method achieved a bit error rate of 10^{-6} at a signal–noise ratio of 46.2 dB under various modulation schemes.**

***Index Terms*—Coherent demodulation, non-flickering communications, optical camera communication (OCC), synchronization, visible light communications (VLC).**

I. Introduction

VISIBLE light communication (VLC) is a new type of wireless communication that uses visible light instead of radio waves as a medium [1]. VLC transmitters send signals by modulating their blinking, so they require light sources with a fast response such as the light-emitting diode (LED) or laser diode (LD). LEDs are commonly used in existing devices such as traffic lights and electronic billboards because of their energy efficiency and low cost [2], [3]. VLC can be divided into two categories based on the light-receiving device: photodiodes and cameras. Photodiode (PD) methods have achieved high communication speeds of over 5 Gbps [4]. However, they are easily affected by light disturbances such as ambient light and other light sources. In contrast, optical camera communication (OCC) is robust against these disturbances because the imaging optics provides a separate reception of light [5], [6]. Moreover, OCC is stable even over long communication distances [6], [7]. The tradeoff is a slower communication speed than for PD methods.

OCC can be divided into two approaches: using a high-speed or specially designed camera, and using a general-purpose camera (e.g., a smartphone camera). As an example of the former, high-speed cameras were used to capture and receive light at 32 kbps [8]. In addition, a specially designed camera was used to achieve a communication speed of 20 Mb/s/pixel [9]. However, high-speed and specially designed cameras are not widely used and are very expensive. In addition, such high speeds require massive computation times for image processing. In contrast, general-purpose cameras have a frame rate of 30–100 fps [10], so their application to OCC has low computational requirements and significantly reduced costs. OCC requires LEDs to blink at a high frequency to avoid flicker that is visible to human eyes in order to reduce health hazards and discomfort [11]. However, low-speed general-purpose cameras do not have a sufficiently fast frame rate to sample such high-speed blinking LEDs. Therefore, developing an OCC method that uses a low-speed general-purpose camera as the receiver without flicker is a significant challenge.

The rolling shutter method and undersampling method have been proposed to reduce the flicker with low-speed cameras [10]. The rolling shutter method exploits the mechanism of rolling shutter-type image sensors, where each pixel line has different exposure timing when capturing an image. This mechanism dramatically increases the sampling rate relative to the frame rate, and the rolling shutter method has been used to achieve communication speeds of over 10 kbps [12], [13], [14]. However, this method requires the light from the LED to be received by many lines of pixels, which limits the size of the light source and the communication distance [15]. The undersampling method uses a pixel value or average of several pixel values per LED in a single image frame. This makes it possible for the camera to receive a signal even when the pixel area of the LED on the captured image is small, and it enables transmission by small light sources and communication over long distances.

Manuscript received 14 December 2022; revised 15 February 2023; accepted 17 February 2023. Date of publication 22 February 2023; date of current version 6 March 2023. This work was supported by JSPS KAKENHI under Grants 20H04226 and 22K19789. *(Corresponding author: Hiroaki Matsunaga.)*

Hiroaki Matsunaga is with the Information Science and Control Engineering, Nagaoka University of Technology, Nagaoka 940-2188, Japan (e-mail: s163211@stn.nagaokaut.ac.jp).

Tomohiro Yendo is with the Electric, Electronic and Information Engineering, Nagaoka University of Technology, Nagaoka 940-2188, Japan (e-mail: yendo@vos.nagaokaut.ac.jp).

Shintaro Arai is with the Electrical and Electronic Engineering, Okayama University of Science, Okayama 700-0005, Japan (e-mail: arai@ous.ac.jp).

Takaya Yamazato is with the Institute of Liberal Arts and Sciences, Nagoya University, Nagoya 464-8601, Japan (e-mail: yamazato@nagoya-u.jp).

Digital Object Identifier 10.1109/JPHOT.2023.3247908

In the undersampling method, the camera is exposed every few LED blinks. There are two main exposure strategies: extremely short and long. An image sensor outputs pixel values by integrating the intensity of the light incident during the exposure time [16], and the handling of this time-integral effect depends on the exposure strategy. The extremely short exposure strategy uses an exposure time of around 1/2000 s, which is sufficiently short that the time-integral effect can be ignored [17], [18], [19], [20]. The camera captures the instantaneous light intensity. The extremely short exposure strategy enables binary phase shift keying (BPSK) and multilevel amplitude shift keying (ASK). However, because less light energy is captured during the exposure, a high-sensitivity image sensor and a high-intensity light source are required. In addition, only the binary phase can be detected, and multilevel phase shift keying (PSK) cannot be used for modulation. In contrast, methods based on the long exposure strategy capture more light energy than the extremely short exposure strategy; for example, UPFSOOK [21] achieved communication at a distance of 160 m with an exposure time of 1/250 s. Furthermore, in previous studies [22], [23] and our own previous work [24], the time-integral effect was utilized to reflect the relationship between the exposure timing and LED blinks as a continuous pixel value to achieve multilevel PSK [24]. Both exposure strategies employ a low-speed camera to capture fast-blinking, and the exposure time is a fraction of the frame period. However, the transmitter has to keep sending a symbol for a frame period or longer because the relationship between the symbol timing of the transmitter and the exposure timing of the receiver is indeterminate. Resolving this indeterminacy will allow the transmitter to send multiple data to different receivers.

In this paper, we propose a new one-to-many time division multiplexing (TDM) method where the exposure timing of the receiver is synchronized with the transmitter. This eliminates the need for the transmitter to send the same symbol for a frame period or longer, so it can instead send time division multiplexed signals of multiple data streams in one frame period. Then, the receiver can select a channel by adjusting its exposure timing. The proposed method achieves multi-stream data multiplexing with no speed reduction compared to the case without multiplexing. Furthermore, while our previous work [24] used two cameras or two light sources, the proposed method uses an LED and a camera, and a single symbol is extracted from a single pixel value in a frame. The advantage of the proposed method is the ability to broadcast on multiple channels. There are various suitable scenarios for employing this method, such as multilingual broadcasting using lighting or electric billboards. The remainder of this paper is organized as follows. Section II describes the modulation and demodulation method as well as the basic principles of the TDM method. Section III describes how the receiver and transmitter are synchronized. Section IV presents experiments performed to evaluate the feasibility of the proposed method, and Section V discusses the experimental results. Section VI concludes the paper. Note that this paper is an expansion of previous papers presented at conferences [25], [26].

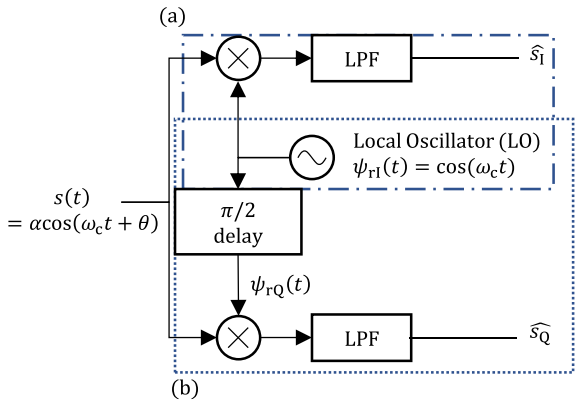

Fig. 1. I/Q demodulator in radio communications. Subset (a) is a coherent demodulator.

II. Principle of the Proposed Method

A. Modulation and Demodulation

In radio communications, in-phase/quadrature (I/Q) demodulation is employed to demodulate high-speed modulated signals and extract low-speed baseband signals. Coherent demodulation is a subset of I/Q demodulation. We previously applied I/Q demodulation to realize flicker-free OCC with multilevel phase and amplitude modulation [24]. In this paper, we present a new OCC method that introduces coherent demodulation so that the receiver can adjust the exposure timing to synchronize with the transmitter and enable TDM.

First, we explain the mechanism of I/Q demodulation. A modulated radiofrequency (RF) signal can be defined as a signal s(t) with an amplitude α and phase that is θ advanced from the carrier signal $\psi_{\mathrm{t}}(t) = \cos(\omega_{\mathrm{c}}t)$:

$$s(t) = \alpha\cos(\omega_{\mathrm{c}}t + \theta) = s_{\mathrm{I}}\cos(\omega_{\mathrm{c}}t) - s_{\mathrm{Q}}\sin(\omega_{\mathrm{c}}t), \quad (1)$$

where t and ω_{c} are the time and angular frequency, respectively. s_{I} and s_{Q} are the in-phase and quadrature components, respectively, of $s(t)$ and are defined as

$$s_{\mathrm{I}} = \alpha\cos(\theta), \quad s_{\mathrm{Q}} = \alpha\sin(\theta). \quad (2)$$

This signal is input to an I/Q demodulator, as shown in Fig. 1. The I/Q demodulator generates a local oscillator (LO) signal $\psi_{\mathrm{rI}}(t) = \cos(\omega_{\mathrm{c}}t)$, whose phase is synchronized with the carrier signal of the transmitter $\psi_{\mathrm{t}}(t)$. This synchronization is called carrier recovery [27]. The signal is shifted by $\pi/2$ rad. to obtain $\psi_{\mathrm{rQ}}(t) = -\sin(\omega_{\mathrm{c}}t)$. Then, the I/Q demodulator multiplies $s(t)$ by $\psi_{\mathrm{rI}}(t)$ and $s(t)$ by $\psi_{\mathrm{rQ}}(t)$, respectively. Next, the signal s'_{I} including the in-phase component s_{I} and the signal s'_{Q} including the quadrature component s_{Q} are extracted:

$$s'_{\mathrm{I}} = s(t)\cos(\omega_{\mathrm{c}}t) = \frac{s_{\mathrm{I}}}{2} + \frac{s_{\mathrm{I}}}{2}\cos(2\omega_{\mathrm{c}}t) - \frac{s_{\mathrm{Q}}}{2}\sin(2\omega_{\mathrm{c}}t), \quad (3)$$

$$s'_{\mathrm{Q}} = -s(t)\sin(\omega_{\mathrm{c}}t) = \frac{s_{\mathrm{Q}}}{2} - \frac{s_{\mathrm{Q}}}{2}\cos(2\omega_{\mathrm{c}}t) - \frac{s_{\mathrm{I}}}{2}\sin(2\omega_{\mathrm{c}}t). \quad (4)$$

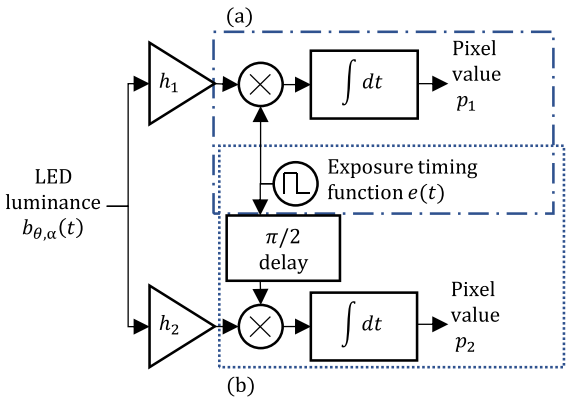

Fig. 2. Our previous I/Q demodulator-based OCC [24] employing two cameras, where parts (a) and (b) correspond to Fig. 1(a) and (b), respectively. The proposed method only uses part (a), which corresponds to a coherent demodulator. h_1 and h_2 are the gains with respect to pixel values.

Then, a low-pass filter (LPF) is applied to remove the high frequency components from s'_{I} and s'_{Q} and extract the signals $\widehat{s}_{\mathrm{I}}$ and $\widehat{s}_{\mathrm{Q}}$, which are proportional to s_{I} and s_{Q}, respectively. Then, $\widehat{s}_{\mathrm{I}}$ and $\widehat{s}_{\mathrm{Q}}$ are used to estimate the phase and amplitude of $s(t)$ [28]. When the received signal is modulated by ASK or BPSK, all of the symbols can be identified from only the in-phase component, so the quadrature component (Fig. 1(b)) can be omitted [28].

Fig. 2 shows our previous receiver, which uses two cameras and is based on I/Q demodulation [24]. A camera corresponds to a coupled multiplier and LPF. The blinking phase and amplitude of a fast-blinking LED are estimated from the pixel values of the LED image. Fig. 3(a) shows the timing relationship between the carrier signal, LED blinking, and exposure. They can be expressed as functions of time. The function of LED luminance is $b_{\theta,\alpha}(t)$. The function of exposure timing is $e(t)$. A square wave $q(t)$ with a duty cycle of 50% is used as the carrier signal instead of a sine wave. $q(t)$ takes values of ± 1. The LED blinks with $b_{\theta,\alpha}(t)$ whose phase is θ and amplitude is α. The phase θ represents how far $b_{\theta,\alpha}(t)$ advances from $q(t)$. $e(t)$ is the exposure function of camera 1 synchronized to the transmitter carrier signal $q(t)$, and is a square wave with the period T_{f} and a duty cycle of 50%, where a value of 1 means exposure and 0 means no exposure. Camera 2 performs the exposure with a delay of $\pi/2$ rad. from $e(t)$. When the images of the blinking LED are captured in a frame period T_{f} that is equal to the blinking period T_{b}, the pixel values p_1 and p_2 vary according to the blinking phase θ and amplitude α as shown in Fig. 3(b).

Our proposed method introduces coherent demodulation to OCC by using only the part in Fig. 2(a), as shown in Fig. 4. Here, $b_{\theta,\alpha}(t)$, $e(t)$, and the time-integral element correspond to $s(t)$, $\psi_{\mathrm{rI}}(t)$, and LPF, respectively, in Fig. 1(a). The relationship between the blinking phase and pixel value can be obtained as follows. The pixel value is proportional to the integral of the incident light during the exposure time. When an LED with the luminance $b_{\theta,\alpha}(t)$ is captured by a camera with the frame period T_{f}, the pixel value p_n of one pixel at a specific position in the

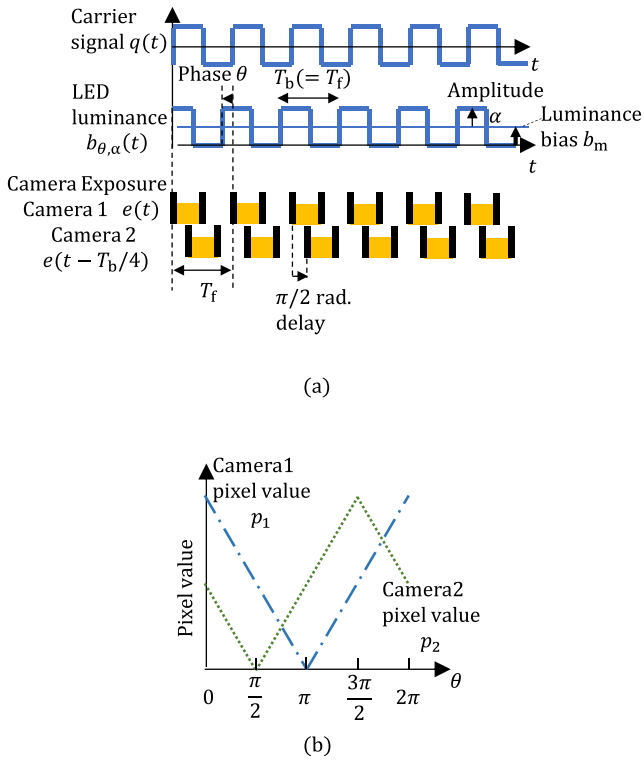

Fig. 3. (a) Waveforms in the I/Q demodulator-based OCC. Exposure is performed when the carrier signal $e(t) = 1$. $e(t)$ is synchronized to the transmitter carrier signal $q(t)$. Camera 2 performs the exposure with a delay of $\pi/2$ from $e(t)$. (b) Relation of pixel values to phase. The phase corresponds uniquely to a pair of pixel values p_1 and p_2.

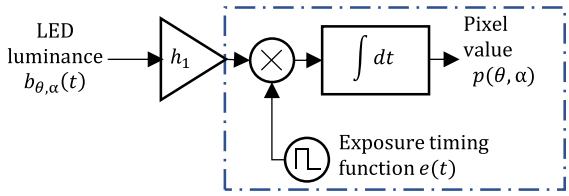

Fig. 4. Structure of the proposed OCC based on coherent demodulation. $b_{\theta,\alpha}(t)$, $e(t)$, and the time-integral element of this model correspond to $s(t)$, $\psi_{rI}(t)$, and LPF, respectively, in Fig. 1(a).

n-th frame can be expressed by [16]

$$p_n = \int_{(n-1)T_{\mathrm{f}}}^{nT_{\mathrm{f}}} h b_{\theta,\alpha}(t) e(t) dt, \tag{5}$$

where h is the proportionality coefficient between the pixel value and luminance value, which depends on properties such as the camera gain and light propagation channel. In this study, we assumed that h is a constant. The exposure function $e(t)$ corresponds to the LO signal $\psi_{\mathrm{rI}}(t) = \cos(\omega_{\mathrm{c}} t)$ for coherent demodulation in RF waves. However, because it represents the opening and closing of the shutter, $e(t)$ is a square wave that only takes values of 0 and 1. Therefore, we use the square wave $q(t)$ as the carrier signal, which only takes values of ± 1 and has

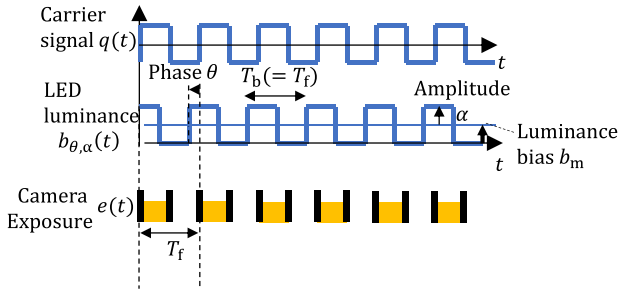

Fig. 5. Relation between the transmitted carrier signal, blinking waveform, and exposure timing in the proposed method.

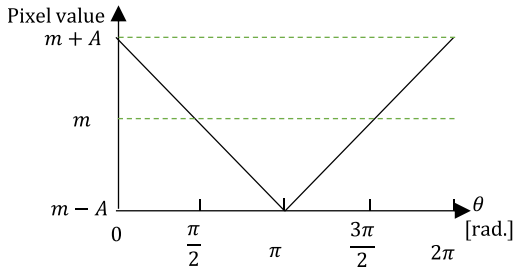

Fig. 6. Relation between the blinking phase and pixel value. m is the pixel value offset and A is the gain coefficient.

a period of $T_b = T_f$ and duty cycle of 50%:

$$q(t) = \sum_k u_{sq}(t - (k-1)T_b), \tag{6}$$

$u_{sq}(t)$ is the unit pulse function and is expressed as

$$u_{sq}(t) = \begin{cases} 1 & (0 \le t \le \frac{T_b}{2}) \\ -1 & (\text{otherwise}) \end{cases}. \tag{7}$$

Carrier recovery is performed so that $e(t)$ and the carrier signal $q(t)$ in the transmitter have the same phases. The exposure function $e(t)$ is expressed as

$$e(t) = \frac{1}{2}q(t) + \frac{1}{2}, \tag{8}$$

and the exposure time per frame $T_e = T_f/2$. Then, the transmission signal is the LED luminance $b_{\theta,\alpha}(t)$, where the amplitude α and phase θ are based on $q(t)$:

$$b_{\theta,\alpha}(t) = \alpha q\left(t + T_b\frac{\theta}{2\pi}\right) + b_m. \tag{9}$$

Here, b_m is the luminance offset to make the LED luminance greater than or equal to 0. Similar to our previous work [24], the relation between the pixel value $p(\theta,\alpha)$ and an LED blinking with the phase θ and amplitude α is given by

$$\begin{aligned} p(\theta,\alpha) &= \int_0^{T_f} h b_{\theta,\alpha}(t)e(t)dt \\ &= \begin{cases} \alpha A\frac{\pi/2-\theta}{\pi/2} + m & (0 \le \theta < \pi) \\ \alpha A\frac{\theta-3\pi/2}{\pi/2} + m & (\pi \le \theta < 2\pi) \end{cases}, \end{aligned} \tag{10}$$

where $A = \frac{hT_f}{2}$ is the gain coefficient and $m = \frac{hT_f}{2}b_m$ is the pixel value offset. Both A and m are constants. Fig. 5 shows a luminance $b_{\theta,\alpha}(t)$ of blinking LED with amplitude α, luminance bias b_m, and its phase is advanced θ from the transmitted carrier signal $q(t)$. The blinking LED is captured according to the exposure function $e(t)$. Then, (10) can be used to obtain the pixel value relative to the phase, as shown in Fig. 6.

In a communications system, a receiver must be able to uniquely identify symbols. From an implementation standpoint, PSK is preferable to ASK for multilevel modulation because the driving circuit can be an ON/OFF driver. Our previous I/Q demodulator-based OCC can uniquely estimate the phase and amplitude from pixel value pairs. However, the phase cannot be uniquely estimated from a pixel value in single camera image because pixel values corresponding to the phase values of θ and $2\pi - \theta$ are the same as shown in Fig. 6 and (10). To estimate the phase uniquely from the pixel value, we limit the phase used in multilevel PSK to the range of 0 to π rad. $\theta_k (k = 0, 1, \ldots, M-1)$ is the phase of the symbols used in M-ary PSK (MPSK) and is given by

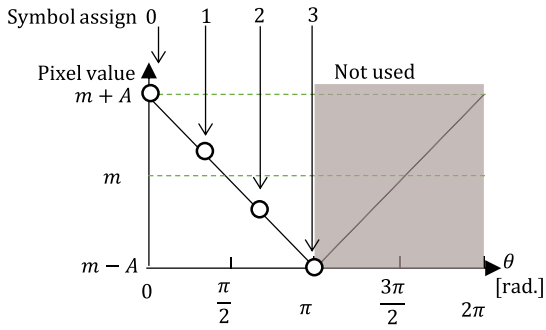

Fig. 7. Example phase assignment and the relationship between the phase and pixel value. In the case of QPSK, the symbols 0,1,2, and 3 are assigned blinking phases of 0, $\pi/3$, $2\pi/3$, and π rad, respectively, and uniquely correspond to pixel values. We set the amplitude $\alpha = 1$ for simplicity.

$$\theta_k = \frac{\pi}{M-1}k, \tag{11}$$

where M is the number of PSK steps. $M = 2$ for binary PSK (BPSK), and $M = 4$ for quadriphase PSK (QPSK). Thus, the pixel value varies linearly with the phase θ_k:

$$p(\theta_k, 1) = A\left(1 - \frac{2}{M-1}k\right) + m. \tag{12}$$

where we set the amplitude $\alpha = 1$ for simplicity. As shown in Fig. 7, the pixel values uniquely correspond to symbols.

B. Flicker-Free Communication and Time Division Multiplexing

The discussion in Section II-A assumes that the frame period T_f is equal to the blinking period T_b. However, if the LED frequency is set to 200 Hz or higher [11] to eliminate flicker, a camera with a frame rate of 200 fps or higher is required. Therefore, according to our previous study [24], we used frame

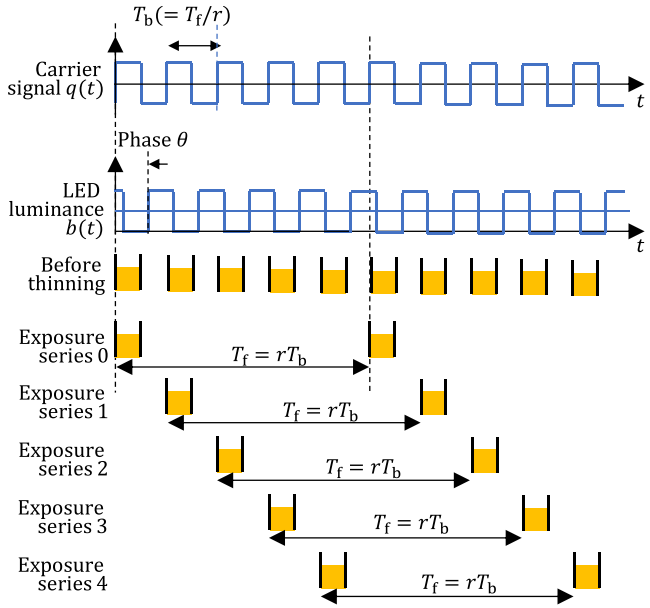

Fig. 8. Relationship between LED blinking and exposure with frame thinning, which can result in an r difference in exposure timing. This figure shows $r = 5$ as an example.

thinning so that the exposure occurs every r blinking, as shown in Fig. 8. This results in a frame period of $T_f = rT_b$, and the phase of a fast-blinking LED can be obtained with a low-speed camera. The exposure time is $T_b/2$, which is the same as the case where the frame period $T_f = T_b$.

With frame thinning, the receiver is only exposed to a fraction of the transmitted signal, and there can be r kinds of exposure series, as shown in Fig. 8. The observed part of the transmitted signal differs depending on the exposure series. Most undersampling OCC methods, including our previous method [24], do not control the exposure timing, so the observed part of the transmitted signal cannot be actively selected. Therefore, to receive a symbol in any exposure series correctly, blinking with the same phase and amplitude must be maintained for T_f or longer. In the present study, the proposed method adjusts the exposure timing so that the observed part of the transmitted signal can be actively selected. As shown in Fig. 8, the receiver can then select one of the exposure series 0–4. This allows TDM to be realized for undersampling OCC, where multiple data streams can be transmitted by switching the phase every blink while taking turns, as shown in Fig. 9. The transmitting signal in one frame period is divided into r periods with a length T_b. These are defined as TDM timeslots, and we can use the same number of channels as the number of TDM timeslots. For each TDM timeslot, PSK is performed as described in Section II-A according to the data of each channel. The period of a timeslot starts at $-T_b/4$ before the rising edge of the carrier signal so that the exposure timing is in the center of the TDM timeslot. We numbered the TDM timeslots $0, 1, 2, \ldots, r-1$ in order from earliest to latest, which are then associated with data on channels $0, 1, 2, \ldots, r-1$.

III. Synchronization Method

Since the exposure timing is undefined at the start of communication, synchronization is necessary. Section II assumes that the exposure function $e(t)$ and transmitted carrier signal $q(t)$ have the same phase. However, if the receiver operates autonomously from the transmitter, a phase difference ϕ occurs between the two signals, as shown in Fig. 10. In this case, the pixel value $p(\theta + \phi, \alpha)$ is obtained for blinking with the phase θ, where ϕ is the phase offset. In our previous I/Q demodulator-based OCC [24], the phase offset ϕ is measured and the phases of received symbols are corrected using ϕ, instead of the carrier recovery. In the present study, we instead synchronize the exposure timing so that $\phi = 0$ before the payload is received. Furthermore, exposure timing should be adjusted to select the TDM timeslot of the desired channel. In the proposed method, the synchronization of the exposure timing has two steps. First, the phase offset ϕ is measured and adjusted so that $\phi = 0$ for the received signal in any TDM timeslot. Next, the exposure timing is adjusted so that the exposure occurs at the TDM timeslot of the desired channel. The two steps are described below.

A. Phase Offset Compensation

1) Mechanism: The receiver estimates the phase offset ϕ by measuring how much the observed phase is shifted in the preamble. However, the phase cannot be estimated uniquely from a single pixel value before synchronization because one pixel value may correspond to two phases. Therefore, to estimate the blinking phase uniquely, the pixel value pair from a pair of frames is used, similar to our previous approach [24]. The LED blinks so that the phase difference is $\pi/2$ rad. in the pair of two frames. As an example, consider the sequence of LED luminance $b(t)$ in Fig. 11. During the first frame period T_f, the LED luminance is b_m. $b(t) = b_m$ corresponds to $\alpha = 0$ and phase cannot be defined. During the second frame period, the blinking phase of the LED is θ_b, and $\alpha = 1$. During the third frame period, the blinking phase of the LED is $\theta_b + \pi/2$, and $\alpha = 1$. The captured pixel value of the first frame p_1 is $p(*, 0) = m$, where $*$ represents an arbitrary phase. In the second frames and third frames, the pixel values p_2 and p_3 are $p(\theta_b + \phi, 1)$ and $p(\theta_b + \phi + \pi/2, 1)$, respectively. By using (10), we can estimate the gain coefficient A from the function $f(p_2, p_3)$:

$$\hat{A} = f(p_2, p_3) := (|p_2 - m| + |p_3 - m|). \tag{13}$$

We can then use $f(p_2, p_3)$ to define the function $g(p_2, p_3)$ for estimating $\theta_b + \phi$:

$$g(p_2, p_3) := \begin{cases} -\frac{\pi}{2}\frac{(p_2 - m)}{f(p_2, p_3)} + \frac{\pi}{2} & ((p_3 - m) \le 0) \\ \frac{\pi}{2}\frac{(p_2 - m)}{f(p_2, p_3)} + \frac{3\pi}{2} & ((p_3 - m) > 0) \end{cases}. \tag{14}$$

Because the blinking phases θ_b in the sequence are known, we can estimate ϕ from p_2 and p_3. We then define the function $v(\theta_b, p_2, p_3)$ for estimating ϕ as

$$\phi = v(\theta_b, p_2, p_3) := g(p_2, p_3) - \theta_b. \tag{15}$$

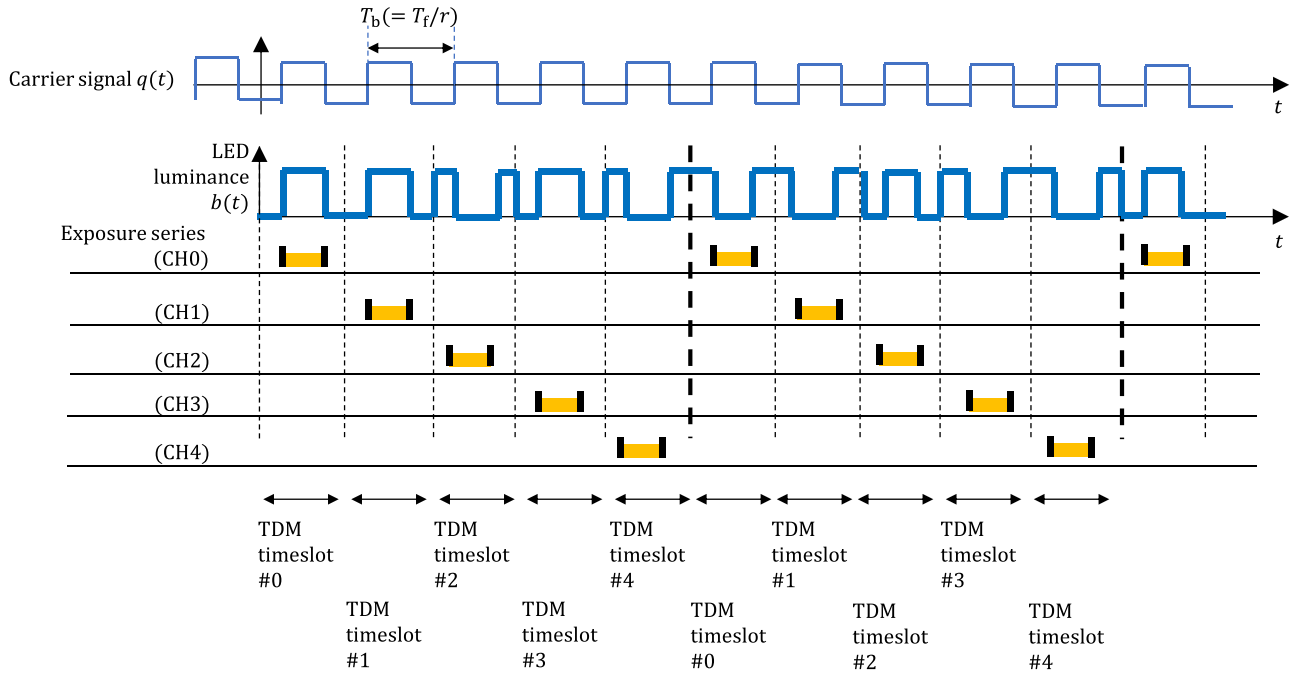

Fig. 9. TDM waveform and exposure series for each channel. This shows $r = 5$ as an example, and five channels of data streams are multiplexed. The data for a desired channel can be obtained by matching the exposure series to the corresponding TDM timeslot.

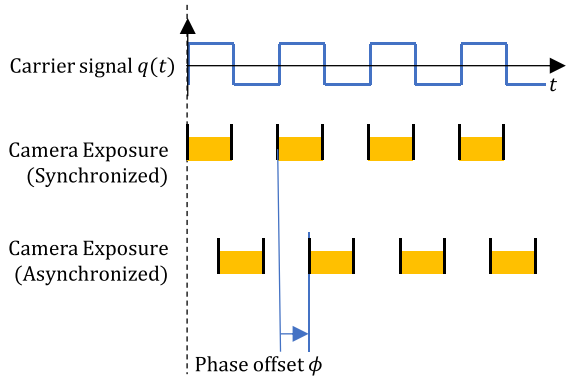

Fig. 10. Phase shift between the transmitted carrier signal $q(t)$ and exposure function $e(t)$. This phase shift is called the phase offset ϕ, and it is defined as positive when the exposure timing is delayed from the synchronized timing.

Thus, it becomes possible to estimate the phase offset ϕ by using a configuration with one LED and one camera. In addition, the gain coefficient A and pixel value offset m necessary for demodulation can be obtained.

2) Estimation of the Phase Offset for Adjustment of the Exposure Timing: The accuracy of estimated phase offset ϕ affects the synchronization accuracy, and A and m are used for demodulation. Thus, the demodulation performance depends significantly on the estimation accuracy of these parameters. Section III-A1 describes how ϕ can be estimated from the blinking pattern of three frames. However, noise in pixel values can cause estimation errors for ϕ, A, and m. The estimation accuracy can be improved by using more frames. Therefore, we use a sequence in which multiple pairs of frames with a phase difference of $\pi/2$ can be made up, as shown in Fig. 12. First, the LED luminance b_{m} for a duration of $4T_{\mathrm{f}}$ is used to obtain m by averaging the four pixel values $p_{\mathrm{m1}}, p_{\mathrm{m2}}, p_{\mathrm{m3}}$, and p_{m4}. Second, four different phases $-\pi/2, 0, \pi$, and $\pi/2$ are used in this order, and the phase offset ϕ is estimated from four pairs of pixel values as

$$\phi = \frac{1}{4}\{v\left(-\pi/2, p_{\mathrm{p1}}, p_{\mathrm{p2}}\right) + v\left(0, p_{\mathrm{p2}}, p_{\mathrm{p4}}\right) + v\left(\pi/2, p_{\mathrm{p4}}, p_{\mathrm{p3}}\right) + v\left(\pi, p_{\mathrm{p3}}, p_{\mathrm{p1}}\right)\}. \quad (16)$$

The gain coefficient A is estimated as

$$A = \frac{1}{4}\{f\left(p_{\mathrm{p1}}, p_{\mathrm{p2}}\right) + f\left(p_{\mathrm{p2}}, p_{\mathrm{p4}}\right) + f\left(p_{\mathrm{p4}}, p_{\mathrm{p3}}\right) + f\left(p_{\mathrm{p3}}, p_{\mathrm{p1}}\right)\}. \quad (17)$$

This blinking sequence is called the phase offset estimation pattern.

Next, the exposure timing is adjusted. As shown in Fig. 13, the frame interval, which is usually the frame period T_{f}, is set as $t_{\mathrm{fd}} = T_{\mathrm{f}} + T_{\mathrm{b}} - \Delta t_{\mathrm{p}}$ for one frame only. Δt_{p} is the time length corresponding to the phase offset ϕ:

$$\Delta t_p = \phi \frac{T_{\mathrm{b}}}{2\pi}. \quad (18)$$

Here, Δt_{p} is less than T_{b}, and the interval t_{fd} is always longer than the frame period T_{f}. We define the frame interval as the time between the start of two consecutive exposures. Note that two error factors need to be considered. The first factor is the

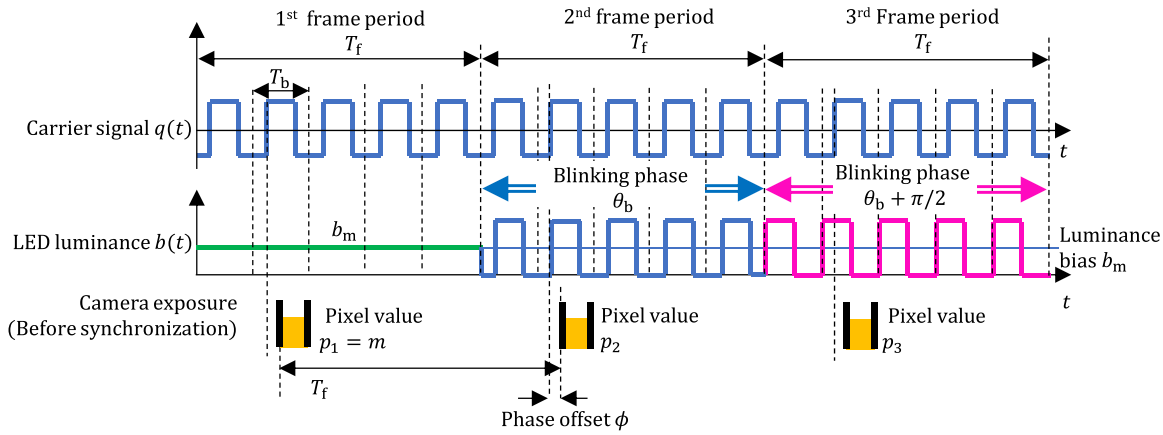

Fig. 11. Example blinking pattern for estimating the phase offset. Exposure is delayed from the rising edge of the carrier signal $q(t)$ corresponding to the phase offset ϕ, and ϕ is estimated from the pixel values p_1, p_2, and p_3.

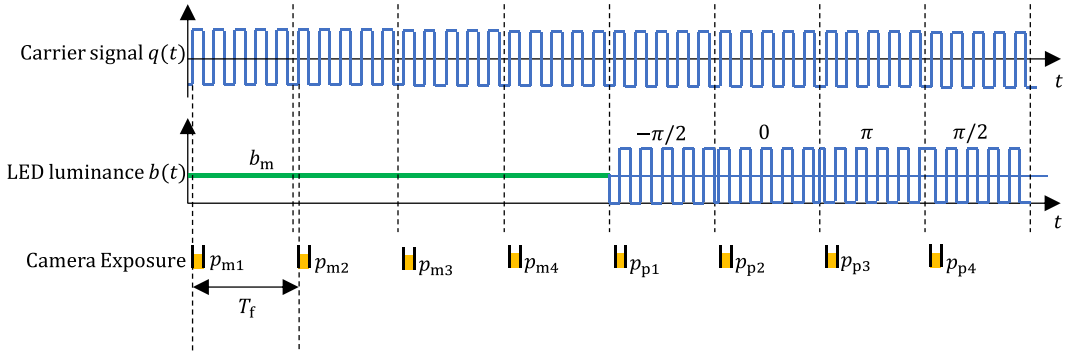

Fig. 12. Phase offset estimation pattern. The LED luminance is b_m for $4T_f$. The LED blinks in four different phases $-\pi/2, 0, \pi$, and $\pi/2$ in this order.

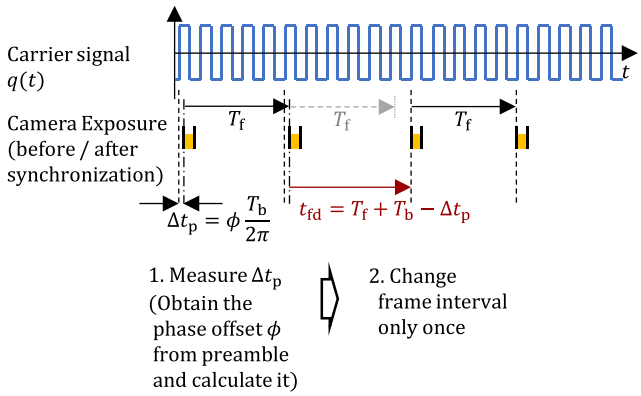

Fig. 13. Adjusting the exposure timing for synchronization. The frame interval is set to $T_f + T_b - \Delta t_p$ instead of the frame period T_f only when the exposure time is adjusted. In this example, the exposure timing is not synchronized in the first and second frames, and the exposure timing adjustment is performed in the third frame.

delay until the effect of adjusting the exposure timing appears. Delays in hardware and software to capture images and adjust the exposure timing mean that the effect only appears several frames later. The second factor is symbol skipping, where a symbol is not captured immediately after exposure timing adjustment. The exposure interval t_{fd} exceeds T_f when the exposure timing is adjusted, and the symbols are transmitted every period T_f. Therefore, a symbol may not be captured depending on the exposure timing.

B. TDM Channel Selection

Section III-A describes how carrier recovery is performed by exposure timing adjustment. However, the channel being received is undetermined. Thus, the receiver needs to identify the channel and adjusts the exposure timing to the desired TDM timeslot. We introduce a blinking pattern called the TDM channel estimation pattern where that the channel number is transmitted in each channel. BPSK is used to transmit three bits of 0, 0, and 0 in channel 0, three bits of 0, 0, and 1 in channel 1, and so on for the other channels. The waveform is shown in Fig. 14. The receiver can use this signal to identify the currently received TDM channel number c_c. The delay time Δt_c is used to adjust the exposure timing for switching to the desired channel number C_d:

$$\Delta t_c = (c_c - C_d)\, T_b. \tag{19}$$

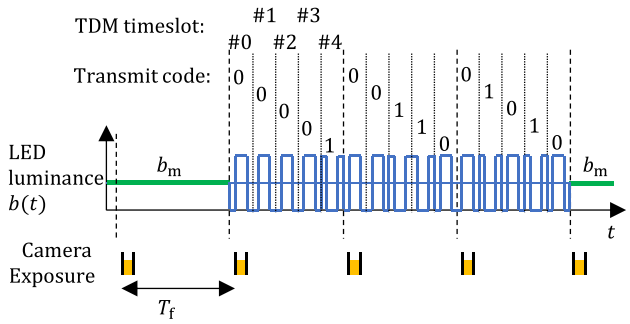

Fig. 14. TDM channel estimation pattern. Because the pixel value offset m has already been obtained, the TDM channel estimation pattern is detected by using the difference in pixel values between m of the dummy symbol and $\pm A + m$ of the BPSK symbol.

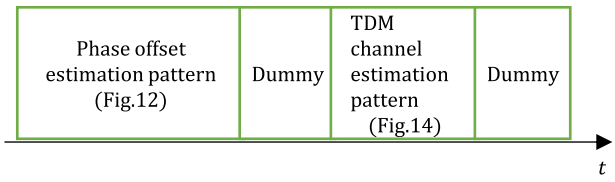

Fig. 15. Proposed preamble structure. Dummy symbols are inserted considering the latency of exposure timing adjustment. The LED luminance is b_m during the dummy symbols.

Then, the exposure timing is adjusted by setting the frame interval, which is usually the frame period T_f, to t_{fd} for one frame only. $t_{fd} = T_f - \Delta t_c$ for $\Delta t_c \leq 0$, and $t_{fd} = 2T_f - \Delta t_c$ for $\Delta t_c > 0$. The latter case causes a symbol skip, which must be considered when the following payload is received. The above procedure allows the receiver to select an arbitrary TDM channel.

To address the potential for operation delay and symbol skipping as mentioned in Section III-A2, an appropriate length of dummy symbols is inserted between the phase offset estimation pattern and TDM channel estimation pattern. During these dummy symbols, the LED luminance is b_m. Then, the receiver detects the TDM channel estimation pattern and obtains the TDM channel. The TDM channel estimation pattern is detected by using the difference in pixel values between m of the dummy symbol and $\pm A + m$ of the BPSK symbol. Because controlling the TDM channel also causes a delay, an appropriate length of dummy symbols needs to be included between the TDM channel estimation pattern and payload. Finally, Fig. 15 shows the proposed preamble structure.

The required dummy symbol length is such that the exposure timing control is finished before the dummy symbols end. The length depends on the receiving system. Considering the mechanism of the camera, basically the receiver system has approximately two frames delay from the exposure trigger to reaching the image data to the processor. The dummy symbol length should be increased if the delay in the system is longer.

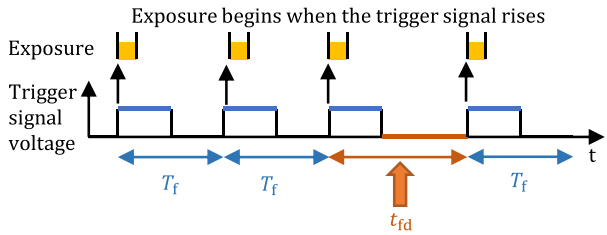

Fig. 16. Exposure timing adjustment using the trigger signal generator. The generator generates trigger pulses whose interval between rising edges is usually T_f. When the PC finishes estimating Δt_p and Δt_c, the trigger signal generator changes once the frame interval t_{fd} corresponds to Δt_p or Δt_c.

IV. Experiment

A. Trigger Signal Generator

Experiments were performed to verify the proposed method. We used a camera whose exposure timing can be adjusted by an external trigger signal and a trigger signal generator that we custom-built. The camera receives an external trigger signal pulse and starts the exposure at the rising edge of the trigger signal, and the duration of the exposure is set by software. The trigger signal generator adjusts the frame period according to a command from a personal computer (PC), which is used for demodulation processing. As explained in Section III, the period of the trigger signal is usually set to the frame period T_f. The time between rising edges is changed to t_{fd} only once when a command comes from the PC, as shown in Fig. 16. The mechanism described in Section III-A2 was designed so that the frame interval t_{fd} is not shorter than T_f to ensure compatibility. In this experiment, the minimum frame interval was set to 19.5 ms, which our camera accepted, instead of $T_f = 20$ ms. The time resolution of the generated trigger signal was 0.5 µs.

B. Experimental Method

We evaluated the proposed method by measuring the signal–noise ratio and bit error rate (SNR-BER) characteristics for different modulation schemes and channels. When communication distance is long or blurring occurs, the received light from the target LED may be attenuated, or disturbing light from the ambient may get mixed. These effects can be treated as SNR varying. To verify the stability of the synchronization, two trigger signal sources were used for the camera: a generated trigger signal in the receiver (generated trigger condition) and an ideal trigger signal supplied from the transmitter (reference trigger condition). Because one frame period was set to five blinks of the LED, the number of TDM channels was set to five. To evaluate the differences among channels, we measured the SNR-BER characteristics using the 8PSK modulation scheme. To evaluate the differences among modulation schemes, we measured the SNR-BER characteristics for the BPSK, QPSK, 8PSK, and 16PSK schemes using only channel 2. The key parameters are presented in Table I. The experimental setup is shown in Fig. 17, and the equipment are listed in Table II. Photographs of the experimental setup and the trigger signal generator are shown

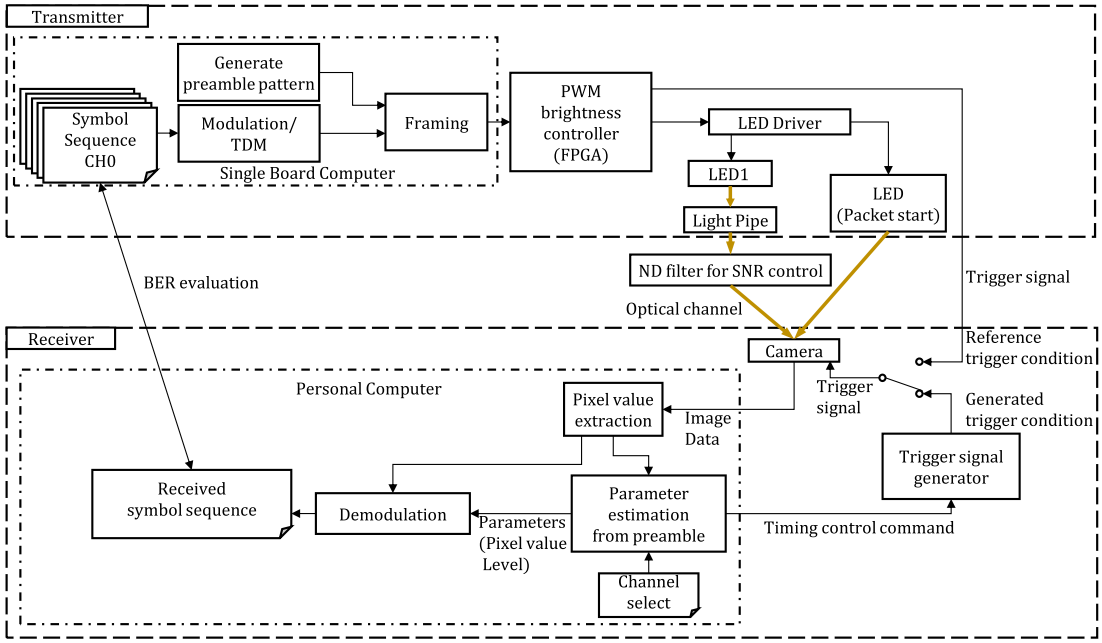

Fig. 17. Block diagram of the communication system used in the experiment.

TABLE I
EXPERIMENTAL PARAMETERS

Modulation Scheme	BPSK, QPSK, 8PSK, 16PSK
LED blinking frequency	250 Hz
PWM frequency	180 kHz
Frame rate	50 fps
Communication distance	1.5 m
Transmitted bit quantity	120 000 bits
Symbol rate	50 symbols per second
Exposure time	2 ms
Lens aperture	F16
Pixel value resolution	12 bits

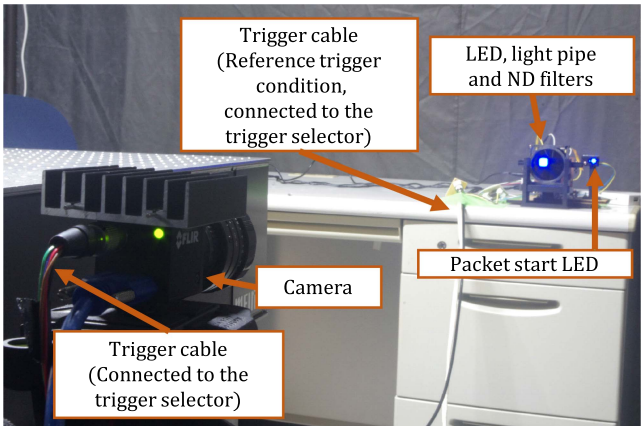

Fig. 18. Experimental setup.

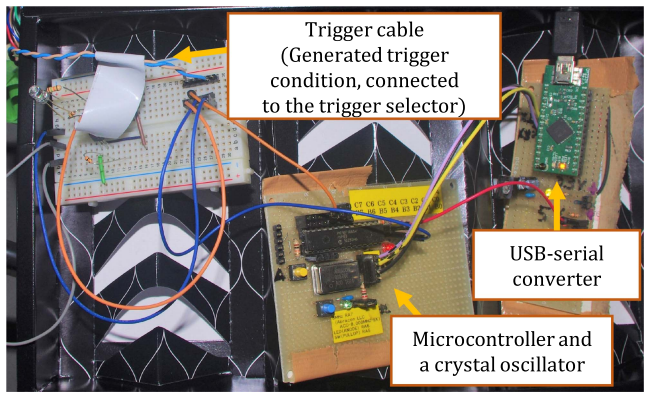

Fig. 19. Trigger signal generator.

in Figs. 18 and 19, respectively. The communication distance was 1.5 m. Experiments were conducted in a dark room.

To vary the SNR, the signal was attenuated by two optical components: the aperture in the lens and the neutral-density (ND) filter stack. The attenuation was controlled by combining ND filters in the stack. The camera gain was set appropriately under these optical attenuations to reduce the quantization error. The ND filter combinations, aperture, and camera gain were adjusted as follows. First, the aperture was set so that the maximum pixel value in 10 s was approximately 85% of the maximum representable value (i.e., 4095) under the conditions that the LED is fully on, the camera gain is 0 dB, and there is no ND filter. This resulted in the F16 aperture condition, which was used in all experiments. Second, we changed the ND filter combination to control the SNR and measured the BER for each ND filter combination. For ND filter combinations I–IV, the camera gain was set so that the maximum pixel value within 10 s was approximately 85% of the maximum representable value to ensure that the pixel value was not saturated and had a small quantization error. For ND filter combinations V and

TABLE II
EXPERIMENTAL EQUIPMENT

Transmitter	
LED	Cree CLP6C-FKB-CK1P1G1BB7R3R3
LED controller	Beagle Bone Black rev. C, Digilent Cmod A7-35T, SN74HC00 (LED driver)
Light pipe	Acrylic rod with dimensions of 10 mm × 10 mm × 100 mm (Wrapped with silver tape and a sanded light exit surface)
ND filters	MARUMI 58 mm NEO MC-ND2, MC-ND4, MC-ND8
	MARUMI 58 mm DHG ND16
	MARUMI 58 mm EXUS ND 32
Receiver	
Camera	FLIR BFS-U3-04S2M
Camera Lens	SPACECOM JHF8M-MP
Microcontroller(Trigger signal generator)	Microchip PIC16F18854
Crystal Oscillator(Trigger signal generator)	Abracon LLC ACO-8.000MHZ-EK
USB to serial converter (Trigger signal generator)	FTDI UM232H
PC	eX. Computer RS7J-D180/T3 (Intel Core i7-8700, 8GB RAM, 240GB SSD, 1TB HDD, Windows 10 Education 21H2)
Luminance meter	Delta OHM HD2302.0 and LP471LUM2 Probe

TABLE III
ND FILTER COMBINATIONS

Index	ND filter combination
I	No filters
II	ND8
III	ND8, ND4, ND2
IV	ND16, ND8, ND2
V	ND16, ND8, ND4, ND2
VI	ND32, ND16, ND8
VII	ND32, ND16, ND8, ND2

beyond, the gain was set to 48 dB, which was the maximum value. Table III presents the ND filter combinations. For the SNR estimation, we captured 10 000 frames of all ND filter combinations with the LED fully on and off. We then calculated the SNR as follows:

$$\mathrm{SNR}\,[\mathrm{dB}] = 20\log_{10}\left(\frac{(\bar{p}_{\max} - \bar{p}_{\min})}{(s_{\max} + s_{\min})}\right), \tag{20}$$

where $\bar{p}_{\max}$ and $\bar{p}_{\min}$ were the average pixel values with the LED on and off, respectively, and $s_{\max}$ and $s_{\min}$ were the standard deviations of the pixel values with the LED on and off, respectively.

In this experiment, we set $\alpha = b_{\mathrm{m}}$ for the LED luminance $b_{\theta,\alpha}(t)$. Thus, the minimum value of (9) was zero (i.e., the LED was turned off), and the maximum value was $\alpha + b_{\mathrm{m}}$ (i.e., the LED was fully on). Therefore, b_{m} was equal to half of the luminance of the LED when it was fully on. Because the proposed preamble includes the lighting portion with the luminance b_{m}, a pulse-width modulation (PWM) with a duty cycle of 50% at 180 kHz, which is high enough for 2 ms exposure, was introduced. To prevent measurement errors due to slight vibrations or misalignment, we attached a light pipe to the front of the LED to make the light exit a uniform surface, and the sum of pixel values in a 5×5 area of the image was used as the pixel value for the demodulation and preamble processing. An acrylic rod wrapped with silver tape and with a sanded light-emitting surface was used as the light pipe. The maximum luminance of the light pipe surface was 575.5 $\mathrm{cd/m^2}$, which was measured from the front at a distance of 100 mm. A photograph of the transmitter is shown in Fig. 20. To detect the beginning of

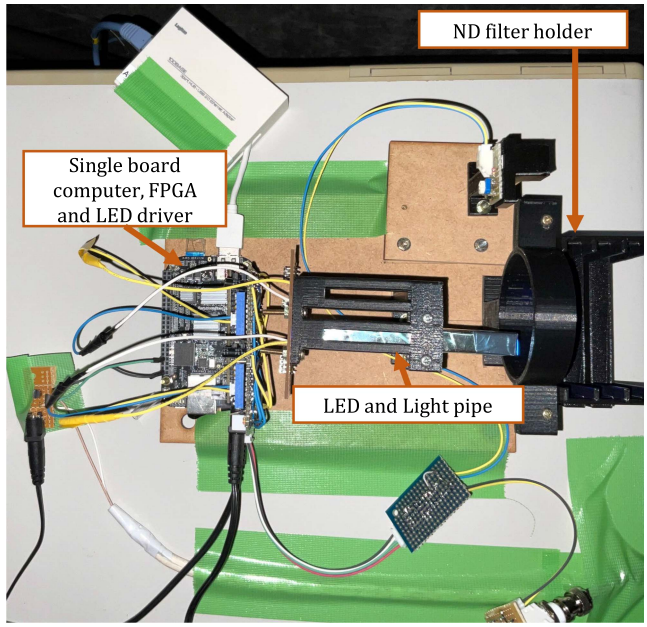

Fig. 20. Transmitter in the experiment.

a packet, an LED that lights up when the first symbol of a packet is transmitted was added. A pseudo-random number sequence of 120 000 bits was generated by the Mersenne–Twister method for each channel and modulation scheme to serve as the transmitted data. To keep the number of bits the same, 120 000, 60 000, 40 000, and 30 000 symbols were used for the BPSK, QPSK, 8PSK, and 16PSK schemes, respectively. We applied Gray codes to assign bits to symbols.

Since the experimental system had two frames delay from the exposure trigger to reaching the image data to the processor, we set the dummy symbols to four frames, including the margin. The payload length was 50 symbols. The payload length was 50 symbols. The packet length was 69 symbols, including the preamble (11 symbols + 4 dummy symbols × 2). Phase offset compensation and TDM channel selection were performed for each received preamble. A dummy packet was inserted at the

TABLE IV
MEASURED SNR FOR EACH ND FILTER COMBINATION

Index	SNR[dB]
I	55.7
II	46.2
III	36.7
IV	30.5
V	22.6
VI	14.4
VII	9.43

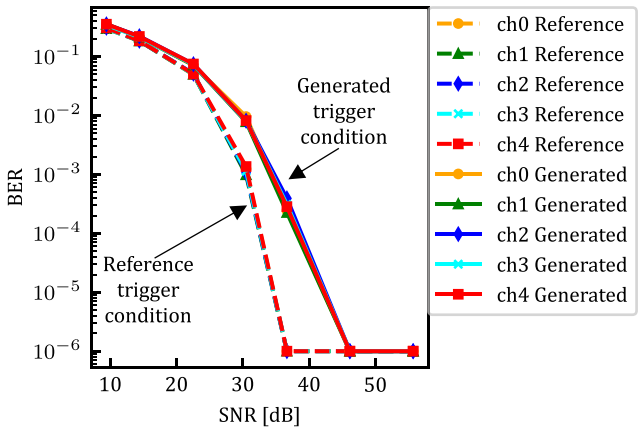

Fig. 21. SNR-BER characteristics with the 8PSK scheme. The reference and generated trigger conditions indicate cases where the signals are supplied from the transmitter and trigger signal generator, respectively. BER 0 was plotted as 10^{-6}. ch0-4 correspond to TDM channels 0–4, respectively.

beginning of each packet, so the number of frames used for communication was 165669 frames for BPSK, 82869 frames for QPSK, 55269 frames for 8PSK, and 41469 frames for 16PSK.

V. RESULTS AND DISCUSSION

Table IV presents the measured SNR for each ND filter combination. Tables V and VI and Fig. 21 present the measured BER for the 8PSK scheme with different TDM channels and ND filter combinations. Table V presents the results under the reference trigger condition, and Table VI presents the results under the generated trigger condition. Fig. 21 graphs the SNR-BER results in Tables V and VI. All channel data were received separately, and Fig. 21 shows that the SNR-BER characteristics for each channel were almost the same. The BER performance in the generated trigger condition was worse than that in the reference trigger condition.

Tables VII and VIII and Fig. 22 present the measured BER in TDM channel 2 with different modulation schemes and ND filter combinations. Table VII presents the results under the reference trigger condition, and Table VIII presents the results under the generated trigger condition. Fig. 22 graphs the SNR-BER data in Tables VII and VIII. The BER values for the 8PSK scheme in Tables VII, VIII, and Fig. 22 were taken from the values of channel 2 in Tables V and VI. No bit errors were obtained for the BPSK, QPSK, and 8PSK schemes under some low-noise conditions. Thus, a BER of 10^{-6} was achieved.

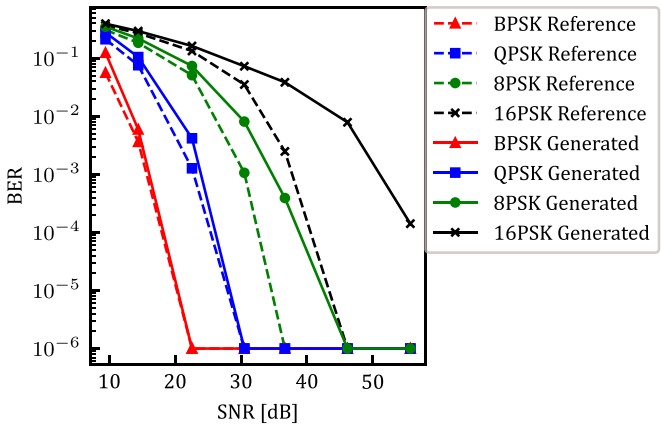

Fig. 22. SNR-BER characteristics in channel 2. BER 0 was plotted as 10^{-6}. The reference and generated trigger conditions indicate cases where the signals are supplied from the transmitter and trigger signal generator, respectively.

Both Figs. 21 and 22 show that the BER performance in the generated trigger condition was worse than in the reference trigger condition. We investigated the causes of errors by graphing the time series of pixel values only in payloads and the pixel value distribution for each transmitted symbol under the generated trigger condition and reference trigger condition. Figs. 23 and 24 show the results for ND filter combinations I and V, respectively. The pixel value distribution for each transmitted symbol was almost the same under the generated and reference trigger conditions. Therefore, we can assume that the trigger signal was generated approximately ideally, which means that the exposure timing estimation and adjustment were performed as expected. The broader distribution of pixel values may be one cause for the greater BER under the generated trigger condition than the reference trigger condition. This broader distribution may be caused by a phase estimation error due to pixel value noise or errors in the frame period and blinking period.

Fig. 25 plots the first and last symbols of each payload for all packets with the 16PSK scheme under the generated trigger condition. The pixel values of the symbols at the end of the payload, which corresponded to the longest time after synchronization, appeared to shift from the pixel values of the first symbols obtained after synchronization. This suggests that the phase offset was shifted in one direction for the last payload symbols compared to the first symbols after the preamble. This may be because the actual trigger signal period T'_{f} was not equal to rT'_{b}, which is the actual blink period T'_{b} multiplied by r, which can be attributed to the inaccuracy of the built-in oscillator in the transmitter and receiver. This difference appeared as a shift of the phase offset in every frame. The proposed method only estimates and adjusts the phase offset measured in the preamble, and it does not consider this period difference. Therefore, adding an algorithm to correct the frame period may reduce the fluctuation of pixel values with respect to the symbols and reduce the BER.

Let us consider the computational cost for demodulation and preamble processing. The proposed method requires real-time pixel value processing to control exposure timing. We employed simple thresholding in the demodulation. For preamble

TABLE V
MEASURED BER FOR DIFFERENT CHANNELS AND ND FILTER COMBINATION WITH THE 8PSK SCHEME UNDER THE REFERENCE TRIGGER CONDITION

Index	Channel (in 8PSK)				
	ch0	ch1	ch2	ch3	ch4
I	0	0	0	0	0
II	0	0	0	0	0
III	0	0	0	0	0
IV	1.23×10^{-3}	9.83×10^{-4}	1.07×10^{-3}	1.13×10^{-3}	1.36×10^{-3}
V	4.89×10^{-2}	4.97×10^{-2}	5.12×10^{-2}	4.95×10^{-2}	5.04×10^{-2}
VI	1.87×10^{-1}	1.83×10^{-1}	1.85×10^{-1}	1.86×10^{-1}	1.85×10^{-1}
VII	3.11×10^{-1}	2.97×10^{-1}	3.08×10^{-1}	2.96×10^{-1}	3.05×10^{-1}

TABLE VI
MEASURED BER FOR DIFFERENT CHANNELS AND ND FILTER COMBINATION WITH THE 8PSK SCHEME UNDER THE GENERATED TRIGGER CONDITION

Index	Channel (in 8PSK)				
	ch0	ch1	ch2	ch3	ch4
I	0	0	0	0	0
II	0	0	0	0	0
III	2.42×10^{-4}	2.25×10^{-4}	3.92×10^{-4}	3.08×10^{-4}	2.83×10^{-4}
IV	9.58×10^{-3}	7.81×10^{-3}	8.13×10^{-3}	8.09×10^{-3}	8.18×10^{-3}
V	7.07×10^{-2}	7.17×10^{-2}	7.39×10^{-2}	7.31×10^{-2}	7.45×10^{-2}
VI	2.16×10^{-1}	2.14×10^{-1}	2.20×10^{-1}	2.13×10^{-1}	2.19×10^{-1}
VII	3.57×10^{-1}	3.50×10^{-1}	3.51×10^{-1}	3.41×10^{-1}	3.53×10^{-1}

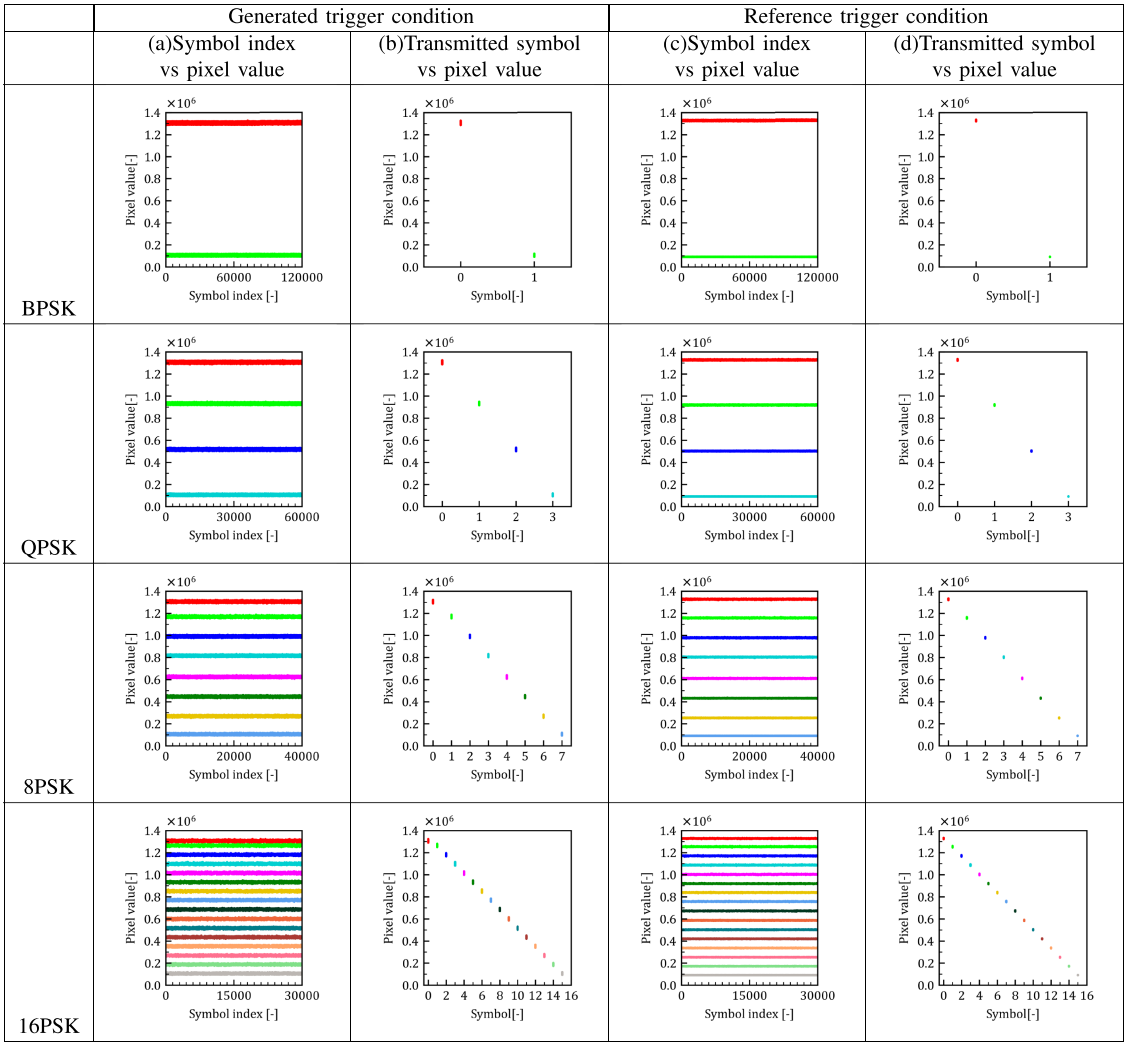

Fig. 23. Graphs of pixel values in payloads for the condition of ND filter combination I and channel 2, plotted in time order and with respect to transmitted symbols.

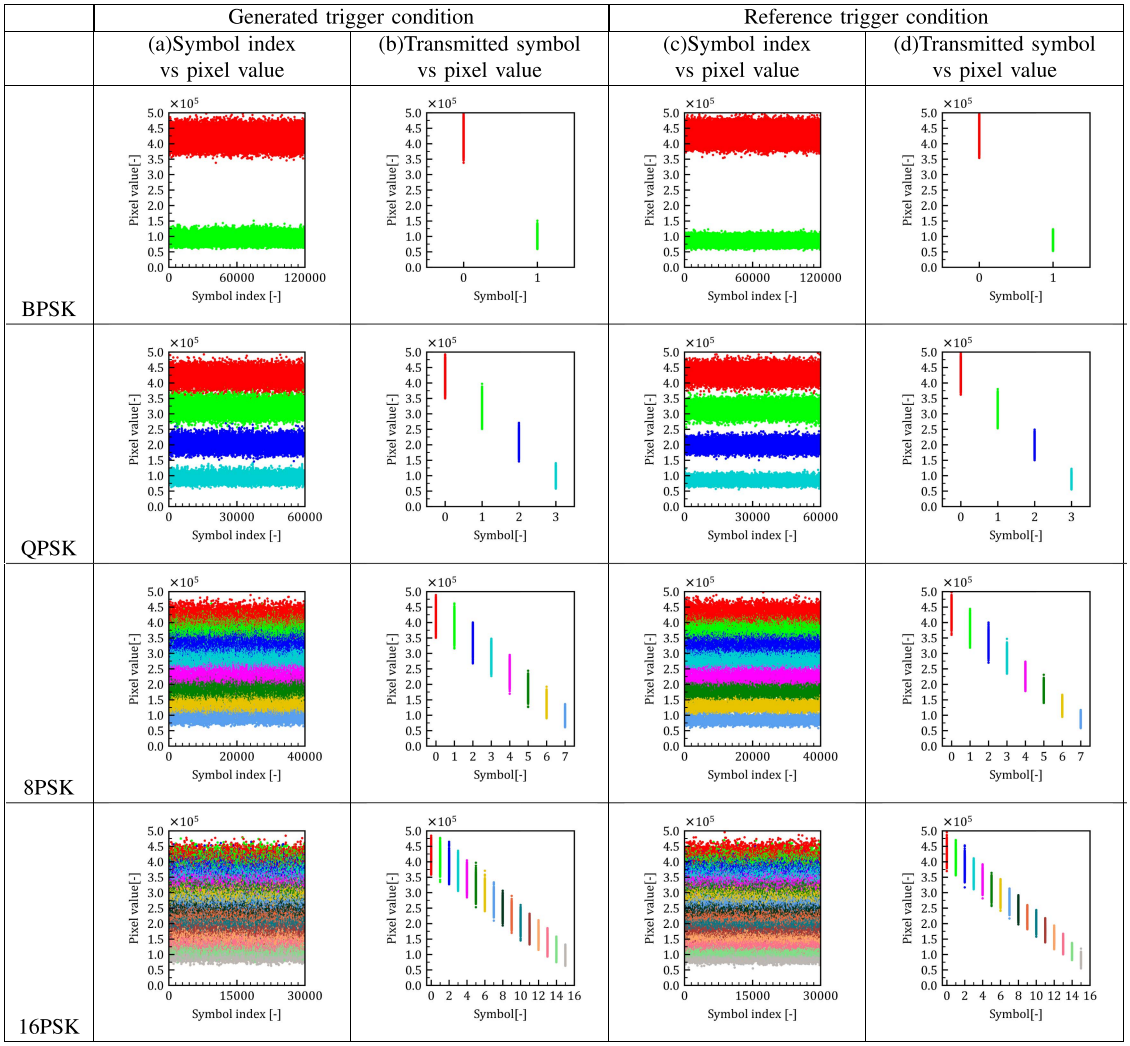

Fig. 24. Graphs of pixel values in payloads for the condition of ND filter combination V and channel 2, plotted in time order and with respect to transmitted symbols.

TABLE VII
MEASURED BER OF DIFFERENT MODULATION SCHEMES AND ND FILTER COMBINATIONS FOR TDM CHANNEL 2 UNDER THE REFERENCE TRIGGER CONDITION

Index	Channel 2			
	BPSK	QPSK	8PSK	16PSK
I	0	0	0	0
II	0	0	0	0
III	0	0	0	2.49×10^{-3}
IV	0	0	1.07×10^{-3}	3.53×10^{-2}
V	0	1.28×10^{-3}	5.12×10^{-2}	1.34×10^{-1}
VI	3.63×10^{-3}	7.61×10^{-2}	1.85×10^{-1}	2.71×10^{-1}
VII	5.65×10^{-2}	2.13×10^{-1}	3.08×10^{-1}	3.66×10^{-1}

TABLE VIII
MEASURED BER OF DIFFERENT MODULATION SCHEMES AND ND FILTER COMBINATIONS FOR TDM CHANNEL 2 UNDER THE GENERATED TRIGGER CONDITION

Index	Channel 2			
	BPSK	QPSK	8PSK	16PSK
I	0	0	0	1.42×10^{-4}
II	0	0	0	7.92×10^{-3}
III	0	0	3.92×10^{-4}	3.87×10^{-2}
IV	0	0	8.13×10^{-3}	7.31×10^{-2}
V	0	4.19×10^{-3}	7.39×10^{-2}	1.63×10^{-1}
VI	5.94×10^{-3}	1.05×10^{-1}	2.20×10^{-1}	2.95×10^{-1}
VII	1.25×10^{-1}	2.78×10^{-1}	3.51×10^{-1}	3.95×10^{-1}

processing, low-latency calculations are required for exposure timing control. The proposed calculation includes 37 addition/subtraction, 11 multiplication/division, 8 absolute value, and 4 conditional branching in the calculation of pixel value offsets and (13)–(17), and 4 addition/subtraction and 4 modulo calculation for phase normalization. Additional calculations are required to generate control commands for trigger control, but this can be accomplished with a few arithmetic operations and conditional branching. The relationship between phase and pixel value is proportional, and threshold values can be calculated from the amplitude and pixel value offset obtained in the preamble. As mentioned above, the computational cost is low enough for real-time processing.

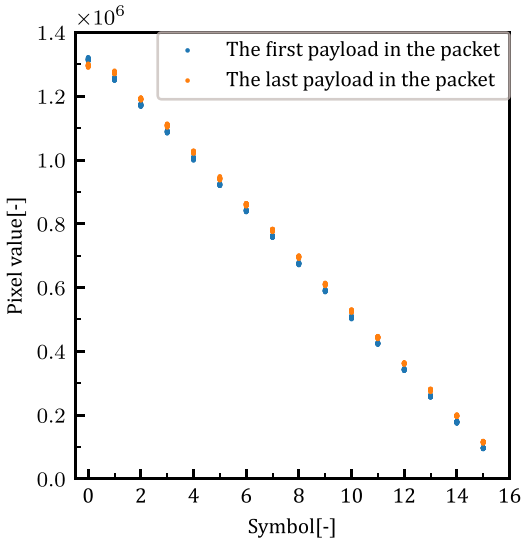

Fig. 25. Transmitted symbol vs. pixel values of the first and last payloads in the packet with no ND filter, the 16PSK scheme, and channel 2 under the generated trigger condition.

To the best of our knowledge, there was no undersampling method with exposure timing control in the past research. In this paper, TDM was realized without reducing the communication speed by controlling the exposure timing. In [22], [24], redundant frames are required to avoid intersymbol interference due to asynchronous communication and it decreases the efficiency. In contrast, the proposed method does not require redundant frames thanks to the exposure synchronization. One weak point of the proposed method is that the trigger signal generator is needed to control the exposure timing. However, it has simple mechanism, so the additional cost of implementation is low.

VI. Conclusion

We proposed a method for flicker-free OCC using a general-purpose low-speed camera. The proposed method employs an undersampling scheme in which the frame period is an integer multiple of the blink period and achieves multiphase modulation by using an exposure time that is half the blinking period. The proposed method utilizes exposure timing synchronization to realize TDM, which enables the transmitter to send multiple data channels in one frame period and the receiver to select one channel, and the ability to demodulate one symbol from one frame using only one LED and one camera. We use the PSK modulation scheme and limit the range of the blinking phase so that phase can be estimated from a single pixel value. To verify the feasibility of the proposed method, we performed experiments and measured the SNR-BER characteristics with different TDM channels and with different modulation schemes. The experimental results confirmed that all channel data were received separately, and a BER of 10^{-6} was achieved with the BPSK, QPSK, and 8PSK schemes under low-noise conditions. The experimental results also suggest that timing errors in the built-in oscillator of the transmitter and receiver caused bit errors. Future work will involve improving the synchronization algorithm to consider oscillator timing errors.

Acknowledgment

This paper was produced by the IEEE Publication Technology Group, Piscataway, NJ.

References

[1] P. H. Pathak, X. Feng, P. Hu, and P. Mohapatra, "Visible light communication, networking, and sensing: A survey, potential and challenges," *IEEE Commun. Surveys Tuts.*, vol. 17, no. 4, pp. 2047–2077, Oct.–Dec. 2015.
[2] M. Akanegawa, Y. Tanaka, and M. Nakagawa, "Basic study on traffic information system using LED traffic lights," *IEEE Trans. Intell. Transp. Syst.*, vol. 2, no. 4, pp. 197–203, Dec. 2001.
[3] T. Komine and M. Nakagawa, "Fundamental analysis for visible-light communication system using LED lights," *IEEE Trans. Consum. Electron.*, vol. 50, no. 1, pp. 100–107, Feb. 2004.
[4] F. Xu et al., "C-plane blue micro-led with 1.53 GHz bandwidth for high-speed visible light communication," *IEEE Electron Device Lett.*, vol. 43, no. 6, pp. 910–913, Jun. 2022.
[5] T. Yamazato and S. Haruyama, "Image sensor based visible light communication and its application to pose, position, and range estimations," *IEICE Trans. Commun.*, vol. E97-B, no. 9, pp. 1759–1765, 2014.
[6] M. Z. Chowdhury, M. T. Hossan, A. Islam, and Y. M. Jang, "A comparative survey of optical wireless technologies: Architectures and applications," *IEEE Access*, vol. 6, pp. 9819–9840, 2018.
[7] M. Shahjalal, M. K. Hasan, M. Z. Chowdhury, and Y. M. Jang, "Future optical camera communication based applications and opportunities for 5G and beyond," in *Proc. Int. Conf. Artif. Intell. Inf. Commun.*, 2019, pp. 492–495.
[8] C. Premachandra et al., "Outdoor road-to-vehicle visible light communication using on-vehicle high-speed camera," *Int. J. Intell. Transp. Syst. Res.*, vol. 13, no. 1, pp. 28–36, Jan. 2015.
[9] I. Takai, S. Ito, K. Yasutomi, K. Kagawa, M. Andoh, and S. Kawahito, "Led and CMOS image sensor based optical wireless communication system for automotive applications," *IEEE Photon. J.*, vol. 5, no. 5, Oct. 2013, Art. no. 6801418.
[10] T. Nguyen, A. Islam, T. Hossan, and Y. M. Jang, "Current status and performance analysis of optical camera communication technologies for 5G networks," *IEEE Access*, vol. 5, pp. 4574–4594, 2017.
[11] "Kookmin university comments to TCD 15-492r2: Flickering consideration for OWC," Accessed Nov. 12, 2022. [Online]. Available: https://mentor.ieee.org/802.15/dcn/15/15-15-0575-01-007a-kookmin-university-comments-to-tcd-15-492r2-flickering-consideration-for-owc.ppt
[12] C. Danakis, M. Afgani, G. Povey, I. Underwood, and H. Haas, "Using a CMOS camera sensor for visible light communication," in *Proc. IEEE Globecom Workshops*, 2012, pp. 1244–1248.
[13] V. P. Rachim and W.-Y. Chung, "Multilevel intensity-modulation for rolling shutter-based optical camera communication," *IEEE Photon. Technol. Lett.*, vol. 30, no. 10, pp. 903–906, May 2018.
[14] C.-W. Chow, Y.-C. Liu, R.-J. Shiu, and C.-H. Yeh, "Adaptive thresholding scheme for demodulation of rolling-shutter images obtained in CMOS image sensor based visible light communications," *IEEE Photon. J.*, vol. 10, no. 6, Dec. 2018, Art. no. 7908506.
[15] P. Luo, M. Zhang, Z. Ghassemlooy, S. Zvanovec, S. Feng, and P. Zhang, "Undersampled-based modulation schemes for optical camera communications," *IEEE Commun. Mag.*, vol. 56, no. 2, pp. 204–212, Feb. 2018.
[16] W. Mao and J. M. Kahn, "Free-space heterochronous imaging reception of multiple optical signals," *IEEE Trans. Commun.*, vol. 52, no. 2, pp. 269–279, Feb. 2004.
[17] R. D. Roberts, "A MIMO protocol for camera communications (CamCom) using undersampled frequency shift ON-OFF keying (UFSOOK)," in *Proc. IEEE Globecom Workshops*, 2013, pp. 1052–1057.
[18] N. Liu, J. Cheng, and J. F. Holzman, "Undersampled differential phase shift ON-OFF keying for optical camera communications," *J. Commun. Inf. Netw.*, vol. 2, no. 4, pp. 47–56, Dec. 2017.
[19] P. Luo et al., "Experimental demonstration of a 1024-QAM optical camera communication system," *IEEE Photon. Technol. Lett.*, vol. 28, no. 2, pp. 139–142, Jan. 2016.

[20] T. Nguyen, A. Islam, and Y. M. Jang, "Region-of-interest signaling vehicular system using optical camera communications," *IEEE Photon. J.*, vol. 9, no. 1, Feb. 2017, Art. no. 7900720.

[21] M. A. Atta and A. Bermak, "A 160 m visible light communication link using hybrid undersampled phase-frequency shift on-off keying and CMOS image sensor," *Opt. Exp.*, vol. 27, no. 3, pp. 2478–2487, Feb. 2019.

[22] S. A. I. Alfarozi, K. Pasupa, H. Hashizume, K. Woraratpanya, and M. Sugimoto, "Square wave quadrature amplitude modulation for visible light communication using image sensor," *IEEE Access*, vol. 7, pp. 94806–94821, 2019.

[23] S. Maruyama, T. Yendo, Y. Shiraki, T. G. Sato, and T. Moriya, "Phase estimation method using multiple frames in image-sensor-based visible light communication," in *Proc. IEEE 16th Annu. Consum. Commun. Netw. Conf.*, 2019, pp. 1–4.

[24] H. Matsunaga, T. Yendo, W. Kihara, Y. Shiraki, T. G. Sato, and T. Moriya, "I/Q demodulator based optical camera communications," *IEEE Photon. J.*, vol. 14, no. 3, Jun. 2022, Art. no. 7324814.

[25] H. Matsunaga and T. Yendo, "Exposure synchronization for resource saved image-sensor-based visible light communication using phase shift keying," in *Proc. 1st Workshop Opt. Wireless Commun.*, 2019, pp. 37–40.

[26] H. Matsunaga and T. Yendo, "Synchronization and multiple access method for optical camera communication using phase shift keying," in *Proc. Conf. IEICE Techn. Committee Submission Syst.*, 2020, pp. 67–72.

[27] K. Feher, *Wireless Digital Communications* (Feher/Prentice Hall Digital and Wireless Communication Series). Englewood Cliffs, NJ, USA: Prentice-Hall, 1995.

[28] A. Goldsmith, *Wireless Communications* (Cambridge Core Series). Cambridge, U.K.: Cambridge Univ. Press, 2005.